F. R. N. Nabarro, Ed. (North Holland, Amsterdam, 1979), vol. 4, pp. 261–362.

4. J. Gil Sevillano, in *Materials Science and Technology*, H. Mughrabi, Ed. (VCH, Weinheim, Germany, 1993), vol. 6, pp. 19–88.

5. R. Madec, B. Devincre, L. P. Kubin, *Phys. Rev. Lett.* **89**, 255508 (2002).

6. P. Franciosi, M. Berveiller, A. Zaoui, *Acta Metall.* **28**, 273 (1980).

7. V. V. Bulatov, F. F. Abraham, L. P. Kubin, B. Devincre, S. Yip, *Nature* **391**, 669 (1998).

8. D. Rodney, R. Phillips, *Phys. Rev. Lett.* **82**, 1704 (1999).

9. V. B. Shenoy, R. V. Kukta, R. Phillips, *Phys. Rev. Lett.* **84**, 1491 (2000).

10. J. L. Bassani, T. Y. Wu, *Proc. R. Soc. London Ser. A* **435**, 21 (1991).

11. E. A. Stach *et al.*, *Philos. Mag. A* **80**, 2159 (2000).

12. M. J. Mills, unpublished data.

13. Methods are available as supporting material on *Science* Online.

14. G. Schoeck, R. Frydman, *Phys. Stat. Sol. B* **53**, 661 (1972).

15. L. K. Wickham, K. W. Schwarz, J. S. Stölken, *Phys. Rev. Lett.* **83**, 4574 (1999).

16. S. Hansen, X. Huang, *Acta Mater.* **46**, 1827 (1998).

17. P. J. Jackson, *Progr. Mat. Sci.* **29**, 139 (1985).

18. E. A. Stach, K. W. Schwarz, R. Hull, F. M. Ross, R. M. Tromp, *Phys. Rev. Lett.* **84**, 947 (2000).

DNA-Templated Self-Assembly of Protein Arrays and Highly Conductive Nanowires

Hao Yan,[1]* Sung Ha Park,[1,2] Gleb Finkelstein,[2] John H. Reif,[1] Thomas H. LaBean[1]*

A DNA nanostructure consisting of four four-arm junctions oriented with a square aspect ratio was designed and constructed. Programmable self-assembly of 4 × 4 tiles resulted in two distinct lattice morphologies: uniform-width nanoribbons and two-dimensional nanogrids, which both display periodic square cavities. Periodic protein arrays were achieved by templated self-assembly of streptavidin onto the DNA nanogrids containing biotinylated oligonucleotides. On the basis of a two-step metallization procedure, the 4 × 4 nanoribbons acted as an excellent scaffold for the production of highly conductive, uniform-width, silver nanowires.

DNA, well known as the predominant chemical for duplication and storage of genetic information in biology, has also been shown to be highly useful as an engineering material for construction of micrometer-scale objects with nanometer-scale feature resolution. Self-assembling nanostructures composed of DNA molecules offer great potential for bottom-up nanofabrication of materials and objects with ever smaller features. Potential applications of DNA self-assembly and scaffolding include nanoelectronics, biosensors, and programmable/autonomous molecular machines. Recently, DNA has been used in the construction of periodically patterned structures (*1–7*), nanomechanical devices (*8–12*), and molecular computing systems (*13–17*). DNA has also been employed, with appropriate attachment chemistries, to direct the assembly of other functional molecules (*18–27*). A variety of unusual DNA motifs (*28*) whose designs are based on the immobile DNA branched junction, a stable analog of the Holliday intermediate from genetic recombination, have been used for self-assembly of periodic or aperiodic arrays (*3–7*).

Here we describe the design and construction of a DNA nanostructure that has a square

aspect ratio and readily self-assembles into two distinct lattice forms: nanoribbons or two-dimensional (2D) nanogrids. The 4 × 4 tile (Fig. 1A) contains four four-arm DNA branched junctions pointing in four directions (north, south, east, and west in the tile plane). It is composed of nine strands, with one of the strands participating in all four junctions. Bulged T_4 loops were placed at each of the four corners inside the tile core to decrease the probability of stacking interactions between adjacent four-arm junctions and to allow the arms to point to four different directions. Although individual branched junctions are expected to be fairly flexible, when constrained by three additional junctions within the tile and a further junction in a neighboring tile, the structure is sufficiently rigid to act as a building block in larger superstructures. Characterization of the annealed structure by nondenaturing gel electrophoresis and thermal transition analysis shows that the 4 × 4 tile is stable and well behaved (fig. S1).

Based on the structure shown in Fig. 1A, two other versions of the 4 × 4 tile with redesigned sticky ends were prepared, assembled, and visualized by atomic force microscopy (AFM) (*29*). By reprogramming the sticky-end associations to vary the assembly strategy, we were able to control the preferred lattice formation. Both designs resulted in lattices containing periodic square cavities.

One strategy (the original design) produced a high preponderance of uniform-width ribbon structures (Fig. 1B). In this design, the distance between adjacent tile centers is an even number of helical half-turns (four full turns) so that the same face of each tile points toward the same lattice face. Figure 1B shows a schematic drawing of the tile and assembly as well as three AFM images of the nanostructures formed from the original design. Self-assembly based on the original design resulted in long (average ~5 μm) ribbon-like lattices with uniform width (~60 nm). The regularity of the periodic cavities is pronounced, as well as the observation that some of the nanoribbons revealed a single-layer flat grid lattice unrolled at the open end of the ribbon. This observation strongly suggests that the ribbon structure results from tube-like structures that flatten when the sample is deposited on mica. The AFM height profile clearly shows that the nanoribbon structure has two layers compared to the flat lattice (fig. S2). Also, the edges of the ribbon appear slightly higher (~0.12 nm) than the middle, indicating a finite radius of curvature for the squashed tube structure (fig. S2). One reason for the formation of tube-like lattices could be that each component tile is designed to be oriented in the same direction in the lattice plane; therefore, any incidental curvature resident in each tile would accumulate and cause circularization of the lattice (see proposed model in fig. S3). This hypothesis is tested and supported by the corrugated design described below.

The second design strategy aimed to eliminate the lattice curvature and produce larger pieces of flat nanogrid with square aspect ratio. This strategy, referred to as the corrugated design, causes adjacent tiles to associate with one another such that the same face of each tile is oriented up and down alternately in neighboring tiles; therefore, the surface curvature inherent in each tile should be canceled out within the assembly (see schematic drawings in Fig. 1C). Figure 1C also includes two AFM images showing the self-assembled lattice with the corrugated design. The designed distance between adjacent tile centers is 4.5 helical turns plus two DNA-helix diameters, totaling ~19.3 nm. The AFM measured distance from center to center of adja-

[1]Department of Computer Science, [2]Department of Physics, Duke University, Durham, NC 27708, USA.

*To whom correspondence should be addressed. E-mail: thl@cs.duke.edu (T.H.L); hy1@cs.duke.edu (H.Y.)

cent tiles is ~19 nm, in good agreement with our design. Large lattice pieces, up to several hundred nanometers on each edge, were observed in which the cavities appeared square. A 2D lattice displaying a square aspect ratio would be useful for forming regular pixel grids for information readout from nanoarrays—for example, by encoding information in a pattern of topographic markers. The large cavities in the 4×4 lattice are bordered by segments of four separate tiles, in contrast with previous parallelogram lattice designs in which the cavities were each defined by a single tile (5, 6). The multi-tile cavities allow for combinatorially defined binding cavities, which may find applications in constructing patterns with addressable features.

One major application of DNA nanotechnology is the use of self-assembled DNA lattices to scaffold assembly of other molecular components. The 4×4 DNA nanogrids have a large cavity size, which may serve as binding or tethering sites for other molecular components. For example, the loops at the center of each 4×4 tile can be modified with appropriate functional groups and used as a scaffold for directing periodic assembly of desired molecules. Here we have used the nanogrids to template streptavidin into periodic protein arrays. We modified the 4×4

DNA tile used in Fig. 1C by incorporating a biotin group into one of the T_4 loops at the tile center. When streptavidin was added to the solution of the self-assembled 4×4 DNA nanogrids, the interaction of streptavidin with biotin led to periodic streptavidin arrays (Fig. 2). Streptavidin has a diameter of ~5 nm, so its binding to the DNA nanogrids generates bumps at the center of the 4×4 tiles (Fig. 2B), which can be compared with regions where there is no streptavidin binding.

We have also used the 4×4 tile assemblies for templating highly conductive metallic nanowires. Bacteriophage λ DNA has been used as a template for the deposition of various metals, including silver (20), gold (21, 22), copper (23), platinum (24), and palladium (25). Here we describe the efficient templating of a conductive nanowire on a self-assembled DNA nanostructure made of synthetic DNA. We have metallized the 4×4 nanoribbons with silver using a two-step procedure (29). The resulting nanowires have been characterized by AFM and scanning electron microscopy (SEM) (Fig. 3; figs. S4 and S5). The metallized nanoribbons have heights of 35 ± 2 nm, widths of 43 ± 2 nm, and lengths of up to ~5 μm (fig. S6). We have patterned metal leads to the wires by electron beam lithography (5-nm Cr followed by 28-nm Au). An SEM image of an actual device

is shown in Fig. 3C. A two-terminal current-voltage (*I-V*) measurement was conducted on this device at room temperature. The *I-V* curve (Fig. 3C, inset) is linear, demonstrating Ohmic behavior in the range of -0.2 to 0.2 V, and the resistance of this sample is 200 ohm as measured between the two central contacts. This
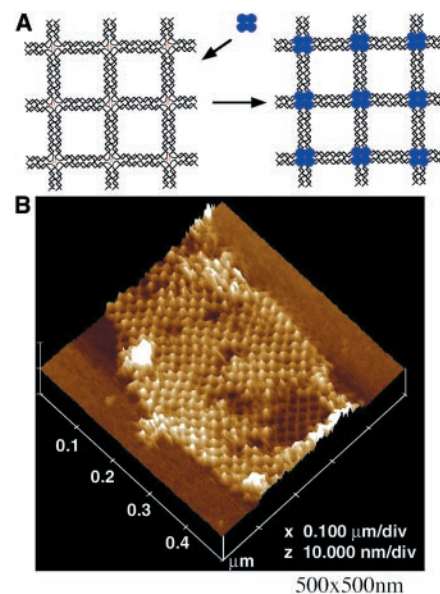

Fig. 2. Self-assembly of protein arrays templated by 4×4 DNA nanogrids. (**A**) Schematic drawing of the DNA nanogrids scaffolded assembly of streptavidin. (Left) The DNA nanogrids, a biotin group labeled as a red letter B, are incorporated into one of the loops at the center of each tile. (Right) Binding of streptavidin (represented by a blue tetramer) to biotin will lead to protein nanoarrays on DNA lattices. (**B**) AFM image of the self-assembled protein arrays; scales are shown below the image.
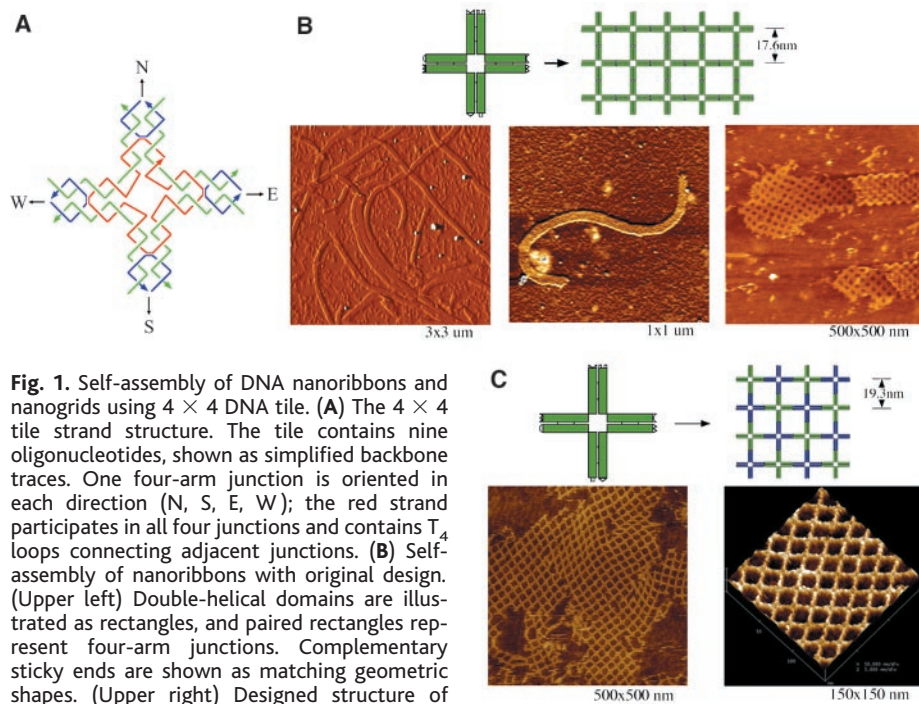

Fig. 1. Self-assembly of DNA nanoribbons and nanogrids using 4×4 DNA tile. (**A**) The 4×4 tile strand structure. The tile contains nine oligonucleotides, shown as simplified backbone traces. One four-arm junction is oriented in each direction (N, S, E, W); the red strand participates in all four junctions and contains T_4 loops connecting adjacent junctions. (**B**) Self-assembly of nanoribbons with original design. (Upper left) Double-helical domains are illustrated as rectangles, and paired rectangles represent four-arm junctions. Complementary sticky ends are shown as matching geometric shapes. (Upper right) Designed structure of self-assembled lattice. (Bottom) AFM images of the nanoribbons. The left panel shows an amplitude-mode image and the right two panels are AFM images in height mode. Scales are shown below each image. (**C**) Self-assembly of 2D nanogrids with corrugated design. (Upper left) The component tile is drawn similar to that in Fig. 1B; positions of sticky ends are changed. The tiles have two surfaces; one faces out of the plane and the other faces into the plane. Here the surface facing out of the plane is indicated in green; the other side (when visible) will be colored blue. (Upper right) Corrugated self-assembly. (Bottom) AFM images of the 2D lattices (nanogrids) formed from the corrugated design. The right panel is a surface plot of a magnified region from the left panel.
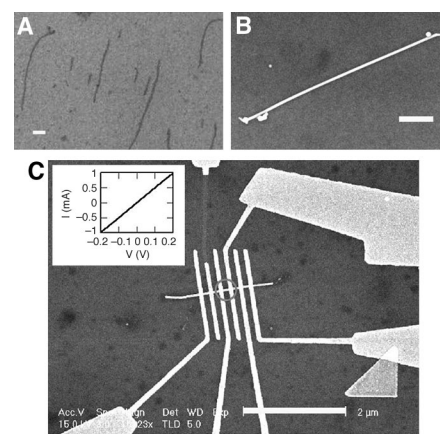

Fig. 3. Metallization and conductivity measurements of metallized 4×4 ribbons. (**A**) SEM image of nonmetallized 4×4 DNA nanoribbons (scale bar: 500 nm). (**B**) SEM image of silver-seeded silver nanoribbon (scale bar: 500 nm). The change in the signal contrast between (A) and (B) is apparent. (**C**) SEM image of the actual device (scale bar: 2 μm). (Inset) Current-voltage curve of the silver-seeded silver 4×4 nanoribbon.

number corresponds to a bulk resistivity of 2.4×10^{-6} ohm·m for the silver nanowire. This nanowire is easily reproducible and has markedly higher conductivity than previously reported double-helix DNA–templated silver nanowires (20).

The 4×4 DNA tile can be easily programmed by varying the sticky ends to form more sophisticated arrays for applications in construction of logical molecular devices; for instance, quantum-dot cellular automata arrays may be constructed by specifically incorporating metal nanoparticles into the nanogrids. The cavities can also be used as pixels in a uniform pixel array, which could be applied to AFM visual readout of self-assembly DNA computations such as a binary counting lattice (30).

References and Notes

1. N. C. Seeman, *Nature* **421**, 427 (2003).
2. T. H. LaBean, in *Computational Biology and Genome Informatics*, J. T. L. Wang, C. H. Wu, P. P. Wang, Eds. (World Scientific, River Edge, NJ, 2003), p. 35.
3. E. Winfree, F. Liu, L. A. Wenzler, N. C. Seeman, *Nature* **394**, 539 (1998).
4. T. H. LaBean *et al.*, *J. Am. Chem. Soc.* **122**, 1848 (2000).
5. C. Mao, W. Sun, N. C. Seeman, *J. Am. Chem. Soc.* **121**, 5437 (1999).
6. R. Sha, F. Liu, N. C. Seeman, *Chem. Biol.* **7**, 743 (2000).
7. H. Yan, T. H. LaBean, L. Feng, J. H. Reif, *Proc. Natl. Acad. Sci. U.S.A.* **100**, 8103 (2003).
8. C. Mao, W. Sun, Z. Shen, N. C. Seeman, *Nature* **397**, 144 (1999).
9. B. Yurke *et al.*, *Nature* **406**, 605 (2000).
10. H. Yan, X. Zhang, Z. Shen, N. C. Seeman, *Nature* **415**, 62 (2002).
11. J. J. Li, W. Tan, *Nano Lett.* **2**, 315 (2002).
12. L. Feng, S. H. Park, J. H. Reif, H. Yan, *Angew. Chem. Int. Ed.*, in press.
13. L. M. Adleman, *Science* **266**, 1021 (1994).
14. Q. Liu *et al.*, *Nature* **403**, 175 (2000).
15. C. Mao, T. H. LaBean, J. H. Reif, N. C. Seeman, *Nature* **407**, 493 (2000).
16. Y. Benenson *et al.*, *Nature* **414**, 430 (2001).
17. B. S. Ravinderjit *et al.*, *Science* **296**, 499 (2002).
18. C. A. Mirkin, *Inorg. Chem* **39**, 2258 (2000).
19. A. P. Alivisatos *et al.*, *Nature* **382**, 609 (1996).
20. E. Braun, Y. Eichen, U. Sivan, G. Ben-Yoseph, *Nature* **391**, 775 (1998).
21. K. Keren *et al.*, *Science* **297**, 72 (2002).
22. F. Patolsky, Y. Weizmann, O. Lioubashevski, I. Willner, *Angew. Chem. Int. Ed.* **41**, 2323 (2002).
23. C. F. Monson, A. T. Woolley, *Nano Lett.* **3**, 359 (2003).
24. W. E. Ford, O. Harnack, A. Yasuda, J. M. Wessels, *Adv. Mater.* **13**, 1793 (2001).
25. J. Richter *et al.*, *Adv. Mater.* **12**, 507 (2000).
26. C. M. Niemeyer, W. Burger, J. Peplies, *Angew. Chem. Int. Ed.* **37**, 2265 (1998).
27. S. Xiao *et al.*, *J. Nanopart. Res.* **4**, 313 (2002).
28. N. C. Seeman, *Trends Biotechnol.* **17**, 437 (1999).
29. Materials and methods are available as supporting material on *Science* Online.
30. E. Winfree, *J. Biomol. Struct. Dyn.* **11**, 263 (2000).
31. We thank E. Winfree, P. Rothemund, and N. Papadakis for helpful advice with AFM under aqueous buffer; D. Liu for development of the metallization procedure and L. Feng for technical assistance in the thermal profile experiment; and J. Liu for providing access to his AFM instrument. This work was supported by grants from the National Science Foundation (H.Y., J.H.R., and T.H.L.) and Defense Advanced Research Projects Agency (J.H.R.) and by an industrial partners arrangement with Taiko Denki Co., Ltd. (J.H.R. and T.H.L.).

Nanoparticle-Based Bio–Bar Codes for the Ultrasensitive Detection of Proteins

Jwa-Min Nam,* C. Shad Thaxton,* Chad A. Mirkin†

An ultrasensitive method for detecting protein analytes has been developed. The system relies on magnetic microparticle probes with antibodies that specifically bind a target of interest [prostate-specific antigen (PSA) in this case] and nanoparticle probes that are encoded with DNA that is unique to the protein target of interest and antibodies that can sandwich the target captured by the microparticle probes. Magnetic separation of the complexed probes and target followed by dehybridization of the oligonucleotides on the nanoparticle probe surface allows the determination of the presence of the target protein by identifying the oligonucleotide sequence released from the nanoparticle probe. Because the nanoparticle probe carries with it a large number of oligonucleotides per protein binding event, there is substantial amplification and PSA can be detected at 30 attomolar concentration. Alternatively, a polymerase chain reaction on the oligonucleotide bar codes can boost the sensitivity to 3 attomolar. Comparable clinically accepted conventional assays for detecting the same target have sensitivity limits of ~3 picomdar, six orders of magnitude less sensitive than what is observed with this method.

The polymerase chain reaction (PCR) and other forms of target amplification have enabled rapid advances in the development of powerful tools for detecting and quantifying DNA targets of interest for research, forensic, and clinical applications (1–3). The development of comparable target amplification methods for proteins could substantially improve medical diagnostics and the developing field of proteomics (4–7). Although one cannot yet chemically duplicate protein targets, it is possible to tag such targets with oligonucleotide markers that can be subsequently amplified with PCR and then use DNA detection to identify the target of interest (8–13). This approach, often referred to as immuno-PCR, allows the detection of proteins with DNA markers in a variety of different formats. Thus far, all immuno-PCR approaches involve initial immobilization of a target analyte to a surface and subsequent detection with an antibody (Ab) with a DNA marker. The DNA marker is typically strongly bound to the Ab (either through covalent interactions or streptavidin-biotin binding). Although these approaches are considerable advances in protein detection, they have several drawbacks: (i) a low ratio of DNA identification sequence to detection Ab, which limits sensitivity, (ii) slow target-binding kinetics because of the heterogeneous nature of the target-capture procedure, which increases

assay time and decreases assay sensitivity, (iii) complex conjugation chemistries that are required to link the Ab and DNA markers, and (iv) PCR requirements (14).

Herein, we report a nanoparticle-based bio–bar-code approach to detect a protein target, free prostate-specific antigen (PSA), at low attomolar concentrations (Fig. 1). PSA was chosen as the initial target for these studies because of its importance in the detection of prostate and breast cancer, the most common cancers and the second leading cause of cancer death among American men and women, respectively (15–18). Identification of disease relapse after the surgical treatment of prostate cancer using PSA as a marker present at low levels (10s of copies) could be extremely beneficial and enable the delivery of curative adjuvant therapies (17, 19). Furthermore, PSA is found in the sera of breast cancer patients, and it is beginning to be explored as a breast cancer screening target (16). Because the concentration of free PSA is much lower in women's serum as compared to that of men, an ultrasensitive test is needed for breast cancer screening and diagnosis.

The bio–bar-code assay reported herein uses two types of probes, magnetic microparticles (MMPs, 1-μm diameter polyamine particles with magnetic iron oxide cores) functionalized with PSA monoclonal antibodies (mAbs) (Fig. 1A) (20) and gold nanoparticles (NP) heavily functionalized with hybridized oligonucleotides (the bio–bar codes; 5' AC-ACAACTGTGTTCACTAGCGTTGAACGT-GGATGAAGTTG 3') (7, 21, 22) and polyclonal detection Abs to recognize PSA (Fig. 1A) (20). In a typical PSA detection experiment (Fig. 1B), the gold NPs and the MMPs sandwich the PSA target, generating a com-

Department of Chemistry and Institute for Nanotechnology, Northwestern University, 2145 Sheridan Road, Evanston, IL 60201, USA

*These authors contributed equally to the work.
†To whom correspondence should be addressed. E-mail: camirkin@chem.northwestern.edu